photonics

MDPI

Article

Multilayer Metamaterials with Vertical Cavities for High-Efficiency Transmittance with Metallic Components in the Visible Spectrum

Huiyu Li, Lin Zhao, Guangwei Chen *, Guoqing Hu and Zhehai Zhou

Key Laboratory of Modern Optoelectronic Measurement Technology in Mechanical Industry, Beijing Information Science and Technology University, Beijing 102206, China; lihuiyu@bistu.edu.cn (H.L.); 2023020239@bistu.edu.cn (L.Z.); guoqing2020@bistu.edu.cn (G.H.); zhouzhehai@bistu.edu.cn (Z.Z.)

* Correspondence: chenguangwei@bistu.edu.cn; Tel.: +86-010-84776417

Abstract: Metasurfaces are opening promising flexibilities to reshape the wavefront of electromagnetic waves. Notable optical phenomena are observed with the tailored surface plasmon, which is excited by metallic components in the visible spectrum. However, metamaterial or metasurface devices utilizing metallic materials encounter the challenge of low transmission efficiency, particularly within the visible spectrum. This study proposes a multilayer design strategy to enhance their transmission efficiency. By incorporating additional metal layers for improvements in the transmission efficiency and dielectric layers as spacers, cavities are formed along the propagation direction, enabling the modulation of transmittance and reflection through a process mimicking destructive interference. An analytical model simplified with the assumption of deep-subwavelength-thick metal layers is proposed to predict the structural parameters with optimized transmittance. Numerical studies employing the rigorous coupled wave analysis method confirmed that the additional metal layers significantly improve the transmittance. The introduction of the extra metal and dielectric layers enhances the transmission efficiency in specific spectral regions, maintaining a controllable passband and transmittance. The results indicate that the precise control over the layers' thicknesses facilitates the modulation of peak-to-valley ratios and the creation of comb-like filters, which can be further refined through controlled random variation in the thickness. Furthermore, when the thickness of the silver layer followed an arithmetic sequence, a multilayer structure with a transmittance of approximately 80% covering the entire visible spectrum could be achieved. Significantly, the polarization extinction ratio and the phase delay of the incident beams could still be modulated by adjusting the geometrical structure and parameters of the multilayer metamaterial for diversified functionalities.

Keywords: transmittance; visible spectrum; metal layer; metamaterial

Citation: Li, H.; Zhao, L.; Chen, G.; Hu, G.; Zhou, Z. Multilayer Metamaterials with Vertical Cavities for High-Efficiency Transmittance with Metallic Components in the Visible Spectrum. *Photonics* **2024**, *11*, 956. https://doi.org/10.3390/photonics11100956

Received: 12 September 2024
Revised: 29 September 2024
Accepted: 9 October 2024
Published: 11 October 2024

1. Introduction

Metamaterials with flexibility in controlling the phase, amplitude, and polarization enable unprecedented manipulation of electromagnetic waves, leading to unattainable applications of natural material [1–3]. Through the unparalleled control approach, various intriguing phenomena, especially the interaction between light and matter at the nanoscale, have been observed [4]. With engineered structures and artificially organized distributions, metamaterials are included in a variety of devices with advanced optical functions, such as metalens [5,6], perfect absorbers [7,8], cloaking, optical coding, and computing [9].

The materials used in metamaterials or metasurfaces primarily include dielectrics, metals, semiconductors, or low-dimensional materials [10–13]. Dielectric materials are typically transparent and exhibit low loss in the visible spectrum. With nanoscale structures, phase delay can be achieved in a planar shape for imaging, focusing, or beam shaping [14]. Tunable metasurfaces and photonic devices for high-density information collection or transmission can be realized by coupling dielectrics with semiconductors or two-dimensional materials [15,16], which are sensitive to environmental conditions and are commonly adopted in the infrared or terahertz spectrum [17–19].

At visible wavelengths, metals can efficiently confine waves along the interface with dielectrics, providing higher stability to enable unprecedented manipulation of electromagnetic waves, leading to applications that are unattainable with natural materials such as hyperbolic material for dispersion modulation, super-resolution imaging through evanescent wave modulation, and subwavelength focusing with super-oscillation, the transmission efficiency of which is less than 0.1% [20–22]. Furthermore, continuous metal films with good conductivity are also necessary for light-emitting devices such as organic diodes, for which, when a silver film is used as an electrode, the transmittance is generally less than 30% [23]. However, the transmission efficiency is low when using plasmonic structures with semiconductors or metallic materials, limiting their applications [24,25].

Researchers are exploring alternative materials and designs to address these limitations, such as hybrid structures that combine metals with low-loss dielectrics [26]. Reducing the total amount of metal used, for example, by incorporating slits, can also help [25]. However, most of these solutions are polarization-sensitive. Meanwhile, developing novel fabrication techniques aimed at reducing defects and optimizing the geometry of individual meta-atoms holds promise for improving the performance of metasurfaces [27]. Therefore, efforts to enhance the transmittance of metamaterials with metal components are required.

High transmission with multilayer structures in the terahertz band has been extensively studied [28]. In simulation models, the metal layer is considered to be a perfect conductor. Unlike in the microwave or terahertz frequency domain, the permeability and permittivity of metals vary in a broader range in the visible spectrum. Thus, the metal components in the metamaterials or metasurfaces cannot be treated as perfect electric conductors, necessitating modifications to the simulation model. In this study, the transmission of a multilayer structure with dielectric and metals was reformed for simulation at visible wavelengths. Meanwhile, the thickness of the metal layers, the dielectric layer, and the cavity between them at the subwavelength scale were considered. Furthermore, a simplified model for designing layered structures with high transmission was proposed, drawing inspiration from antireflection coatings and the blue- or red-shift phenomenon of hyperbolic structures [1,29], with which the thicknesses of both the metal and dielectric layers were in deep subwavelengths, resulting an ultra-low transmittance. The numerical results were compared with those calculated via rigorous coupled wave analysis methods. The simulation results demonstrated that by manipulating the thickness and permittivity of the inner layers, transmission can be significantly improved with the assistance of vertical cavities and surface plasmon coupling. Additionally, with proper hole or slit structures within the multilayer configurations, phase delay and the polarization direction can be precisely controlled, offering an alternative approach to designing metalenses or polarizers with enhancements.

2. Theoretical Analysis and Simulation Methods

A schematic diagram of the multilayer structure featuring both high transmittance and a metallic layer is depicted in Figure 1b. The multilayer structure is situated on a glass substrate, a common choice for supporting metal films in the visible spectrum. When incident light in the visible spectrum passes through the metal film, the intensity is sharply attenuated. However, if the thickness of the metal film is at a deep subwavelength scale, some light can penetrate the film. In our design, a dielectric film with high transmittance in the visible spectrum is employed to compensate for phase delay, mimicking an antireflective coating. Therefore, the transmission can be enhanced with additional metal layers by leveraging the principles of thin-film interference and antireflective coatings.

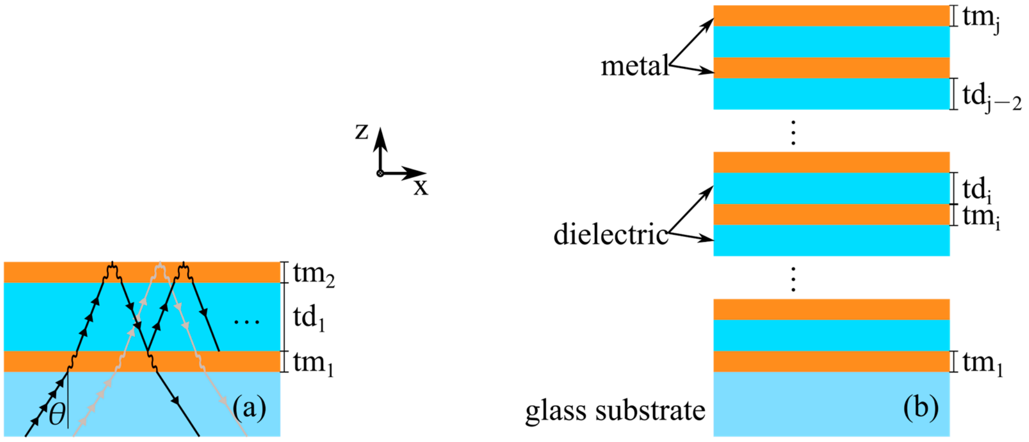

Figure 1. Schematic for the theoretical analysis and numerical simulation: (**a**) multiple reflections and interferences among the beams at different position (line with different color as an example) within the metal–dielectric–metal layer structure; (**b**) The multilayer structure.

A theoretical model was initially established to predict the parameters that can amplify transmission. According to Maxwell's equations, a plane wave can be described as:

$$\vec{E}_{d,m} = \vec{A}_{d,m} exp[i(\vec{k}_{d,m} \cdot \vec{r}_{d,m} - \omega t)] \tag{1}$$

The subscripts d and m denote the wave propagating in the dielectric and metal layers, respectively; k is the wave number; and ω is the angular frequency. For the dielectric and metallic material, k is expressed differently:

$$k_d = 2\pi n/\lambda \tag{2}$$

$$k_m = \omega\sqrt{\varepsilon\mu}\left[\frac{1}{2}\left(\sqrt{1+\frac{\sigma^2}{\varepsilon^2\omega^2}}+1\right)\right]^2 + i\omega\sqrt{\varepsilon\mu}\left[\frac{1}{2}\left(\sqrt{1+\frac{\sigma^2}{\varepsilon^2\omega^2}}-1\right)\right]^2 \tag{3}$$

Here, n is the refractive index of the dielectric material; ε, μ, and σ are the permittivity, permeability, and conductivity of the metallic material, respectively. The phase delay of light during a single reflection cycle within the dielectric layer can be predicted with a general equation

$$p_{di} = 2k_d t_{di} cos\ \theta \tag{4}$$

where θ is the incident angle from the glass substrate to the multilayer structure, considering a simplified multilayer structure with a single dialectic layer sandwiched between two metal layers, as shown in Figure 1a. The phase delay in the metal layer calculated with a simplified equation is suggested in our study. Given the deep subwavelength thickness of the metal film, the effects of attenuation and free electron motion are negligible, and the refraction angle is approximated to zero. Thus, the component of $cos\ \theta$ is degenerated to 1 [1,28]. Furthermore, a correction factor of n_m/n_d is introduced to account for the excitation of the surface plasmon polaritons at the dielectric–metal boundary when illuminated with visible light. For a subcomponent layer composed of a metal–dielectric–metal structure, the transmission reaches a maximum when the phase delay is a multiple of π upon reaching the boundary between the lower metal film and the dielectric film after reflection by the upper metal film. Under this condition, the reflection decreases to zero due to destructive interference. Therefore, the phase delay in the subcomponent of the two-metal layer structure given by:

$$p_{mi} = k_m \cdot (t_{mi}\frac{2n_{mi}}{n_{di}+n_{di-1}} + t_{mi+1}\frac{n_{mi}}{n_{di}} + t_{mi+1}\frac{n_{mi}}{n_{di+1}}) \tag{5}$$

The thicknesses of the metal and dielectric layers are denoted by tm_i and td_i, respectively. The total number of the metal layers, j, defines the layer number of the whole structure.

The equation is given considering the transmission of the upper layer and the destructive interference at the upper side of the lower layer. Thus, the transmittance of the layered structure can be improved by adding additional metal layers, and the parameters can be approximately predicted when the thicknesses of the metal and dielectric films satisfy the following equation:

$$\sum_{i=1}^{n} 2\left(p_{di} + p_{mi} + \frac{tm_{i+1}}{\lambda}\pi\right) = \pi(2l+1),\ \ l = 0,\ 1,\ 2\ \ldots \tag{6}$$

This simplified equation applies only when the metal film is at a deep subwavelength thickness, where the phase retardation becomes more complex and requires modification. The parameters needed to enhance the transmission efficiency of structures with metal components by adding dielectric attachment layers can be roughly predicted using Equation (6). Our previous results showed that the transmission of layered structures at subwavelength scales calculated under these assumptions via the rigorous coupled wave analysis (RCWA) method [30,31] and the permittivity derived from the Johnson and Christy model [32] aligned well with the experimental data [21,33,34], which were adopted in the simulation in this work. The multilayer structure is isotropic along the surface perpendicular to the incident wave. Therefore, the transmittance remains unchanged with the polarization direction, and a circularly polarized incident light was assumed.

3. Simulation Results

This section presents numerical simulations of structures using typical parameters based on current fabrication capabilities to validate the proposed predictive equations and optimize transmittance. The thickness of the continuous metal film can be reduced to 0.5 nm [35]. However, for practical considerations and to ensure adequate performance and stability, the minimum thickness of the metal layer was set to 5 nm. Silver was selected as the metal layer due to its high conductivity and widespread use in organic laser diodes. The refractive index of the dielectric layer was set to 1.43, corresponding to materials such as magnesium fluoride or spin-on glass, which can be fabricated using established techniques such as evaporation or spin-coating, ensuring compatibility with existing manufacturing processes. The structures were placed on a glass substrate with a refractive index of 1.46, providing a stable base for the layered configuration. These parameters were chosen to balance practical fabrication constraints with optimal transmissivity, thereby facilitating the validation of the theoretical predictions.

3.1. Transmittance of the Silver–Dielectric–Silver Layer

To test the prediction of the proposed equations in a simplified mode, simulations of a multilayer structure with j = 2, resulting in a metal–dielectric–metal sandwich structure, were carried out, as presented in Figure 1. The simulations were conducted at a wavelength of 640 nm with normal incidence, and the transmittance of the single metal layer was plotted in the figure as a control. With variations in the thickness of the dielectric and bottom silver layers, high transmittances were observed, as shown in Figure 2a. The red dashed lines represent calculations using Equation (6) with different phase levels. A good match between the numerical simulations and the analytical equation is evident. However, there is a slight positional offset due to the simplification in the phase jump calculation between the dielectric and metal layers and the omission of the multireflection between the metal and dielectric layers. This simplification ignores the influence of free electrons and multireflections between different layers. Thus, the equation is best suited for thin metal films.

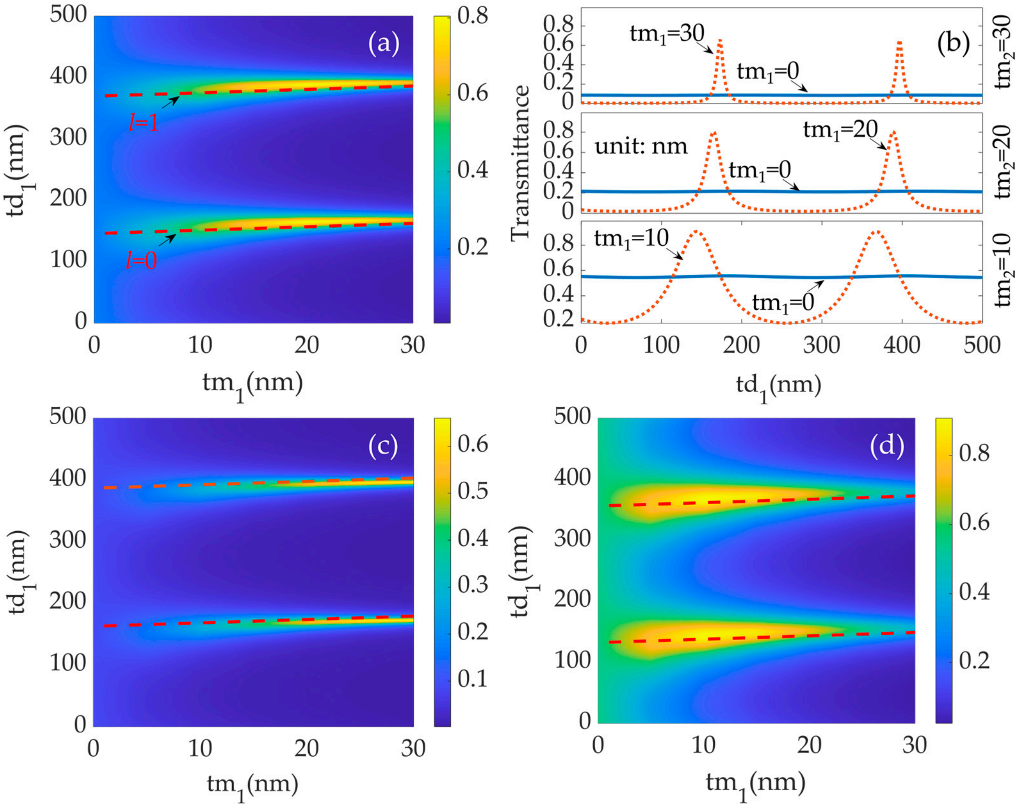

Figure 2. Transmittance of the silver–dielectric–silver film. (**a**) Variance in transmittance with the thickness of the dielectric layer with tm_2 = 20 nm; the red dashed line was calculated with Equation (6). (**b**) Comparison of transmittance between single and double metal layer structures, depending of the thickness of the dielectric layer. The insets are the transmittance distribution, depending on the dielectric and metal layers with the corresponding thickness, as well as the analytical prediction. (**c**) and (**d**) Variance in transmittance with the thickness of the dielectric layer with tm_2 = 30 and 10 nm, respectively; the red dashed line was calculated with Equation (6).

Additionally, the intensities of the transmittance increase and then decrease with increasing tm_1 when $tm_2 = 20$ nm. The maximum transmittance occurs at $tm_1 = 20$ nm, which aligns with the principle of antireflection films. Furthermore, transmittance enhancement is more significant with increased thickness of the silver film, as demonstrated in Figure 2b, where both single and double silver layer structures are plotted. A slight variation in transmittance could be observed for the single silver film; this was due to the destructive interference of the dielectric film on top of the silver layer. The variation trend agrees with classical coating techniques of antireflection coating. Enhancements ranging from two- to four-fold can be achieved. For the transmittance of the single silver film, subtle fluctuations occur with the thickness of the dielectric layer due to the formation of a cavity between the substrate and the silver layer, influencing transmittance through boundary interference. Beyond transmittance enhancement, the overall transmittance decreases with the total thickness of the metal layer. In the proposed structure, transmittance is improved by adding a dielectric layer to form cavities, and this can be further enhanced by increasing the number of layers.

Figure 3a further illustrates the wavelength-dependent transmission when $tm_1 = tm_2 = 20$ nm. Transmittance varies with the thickness of the dielectric films due to destructive interference. However, transmittance decreases sharply due to constrictive interference and the inherent low transmittance of the metallic material, making the structure suitable for applications requiring high absorption or reflection as well. The transmittance is higher at smaller wavelengths, and the slope of the transmittance line increases with the phase level l, which can be used to narrow the passband.

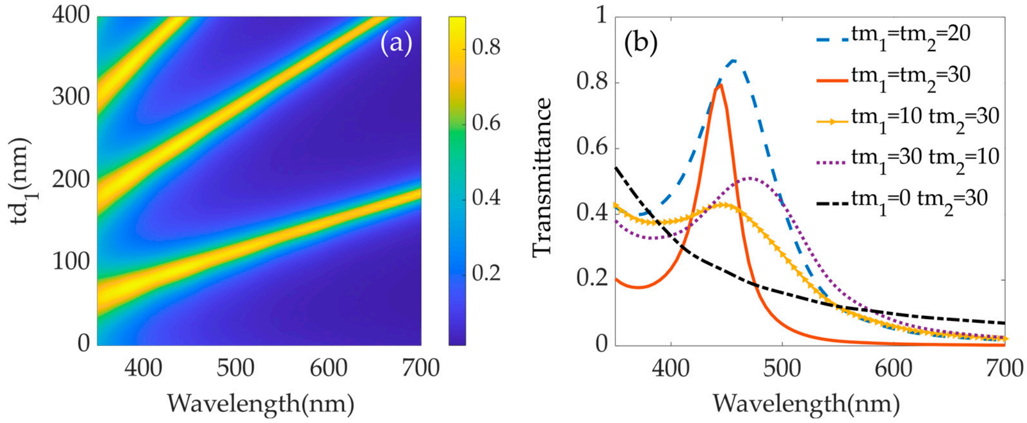

Figure 3. Transmittance of the silver–dielectric–silver film, depending on (**a**) the thickness of the dielectric layer with $tm_1 = tm_2 = 20$ nm. (**b**) Comparisons with different thicknesses of the metal film at td = 100 nm.

The thickness of the metal film plays a critical role in refining the bandwidth of the transmittance. The full width at half maximum (FWHM) decreases with the increasing thickness of the metal film. For a structure with a consistent silver film thickness, the FWHM reduces from 100 nm at $tm = 20$ nm to 40 nm at $tm = 30$ nm. The transmittances for various thicknesses of the silver layer are depicted in Figure 3b. The introduction of an additional metal layer enhances the transmittance. Specifically, the transmittance is enhanced fourfold by adding a 30 nm thick silver layer to reach 80%. Although the thickness of the top silver film increases by 50%, from 20 nm to 30 nm, the reduction in transmittance is less than 6% due to the presence of the additional bottom layer. An intriguing observation is that exchanging the thicknesses of the two metal layers in the multilayer structure alters the transmittance and peak position, effectively rendering the structure bifacial, as exemplified by the films with thicknesses of 10 nm and 30 nm.

Moreover, the incident angle significantly influences the optical path within the dielectric film. The transmittance at a wavelength of 640 nm, as a function of the incident angle θ, is illustrated in Figure 1. The red curves correspond well with the transmittance peaks obtained from numerical simulations, as shown in Figure 4a. However, the transmittance diminishes to zero when the incident angle exceeds 42°, resembling the phenomenon of total internal reflection. Increasing the metal film's thickness to 30 nm results in splitting the transmission enhancement line as the incident angle increases. When the metal layer thickness is not within the deep subwavelength region, the influence of both long-range and short-range surface plasmons becomes more pronounced, necessitating a modification of the linear assumption used in Equation (6).

3.2. Transmittance of a Triple Silver Layer Structure

The transmission peak is intrinsically linked to the thickness of each layer within the structure. A multilayer structure with $j = 3$ was examined as an example to investigate the impact of the parameters on the transmittance. In this three-layered configuration, the additional dielectric and metal layers provide additional parameters to modulate the incident field. The totality of the parameters available in the five-layer structure provides a greater variety of combinations. One significant advantage of this configuration is the ability to modify the transmission line into a curved form, as demonstrated in Figure 5a with $td_1 = 400$ and tm = 10, 20, and 15 nm. Consequently, a double-peak transmission curve can be achieved, featuring uniform transmittance but varying peak separations, as illustrated in Figure 5b with $td_1 = td_2 = td$. The transmittance, peak position, and the distance between the peaks are all directly influenced by the thickness of each layer.

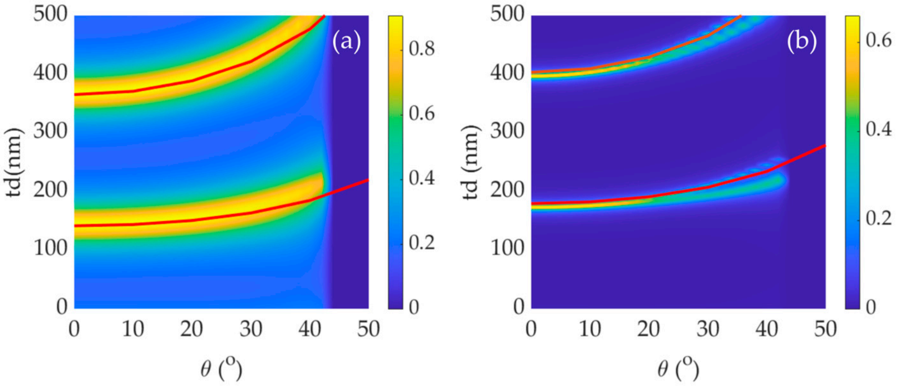

Figure 4. Transmittance of the silver–dielectric–silver film, depending on the incident angle. The red lines in the figure were calculated with the analytical simplified equation: (**a**) tm = 10 nm; (**b**) tm = 30 nm.

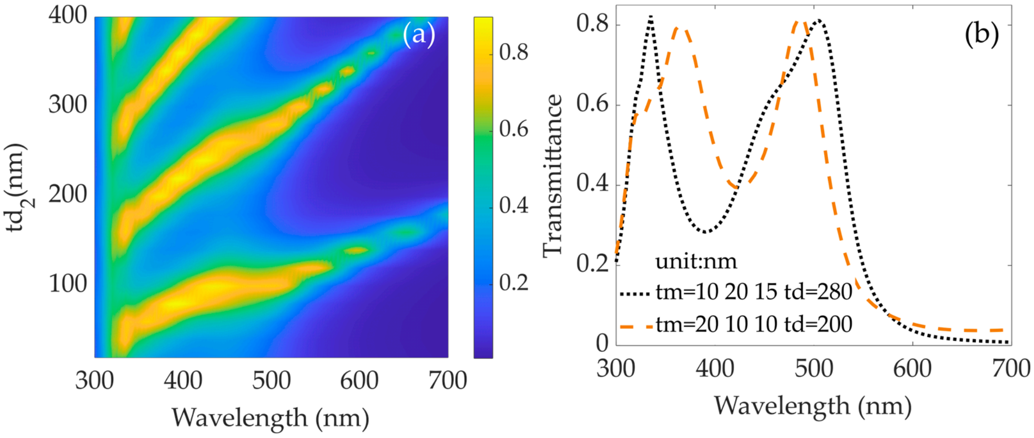

Figure 5. Transmittance of the multilayer structure with n = 3: (**a**) td_1 = 400 nm, tm = 10, 20, and 15 nm; (**b**) double-peak transmittance with td_1 = td_2 = td.

Alternatively, the characteristics of transmittance can be further tailored by reducing the thickness of either the first or second layer and treating the subcomponent as an effective medium. Unlike the metal layers, varying the thickness of the dielectric layer produces a symmetrical pattern relative to the diagonal, as illustrated in Figure 6. Similar to the behavior observed in the two-layered structure, the highest transmittance is achieved when the thicknesses of the metal layers are equal.

3.3. Transmittance of Multilayer Structures

Adding metal and dielectric layers can further modulate the passband, peak number, and peak position. As depicted in Figure 7a, the transmittance distribution varies with an increasing number of silver layers. The dielectric and silver layers' thicknesses are equal for simplicity and ease of comparison. As the number of layers increases, the cumulative thickness of the silver layers also increases, leading to a general decrease in transmittance. Notably, high transmittance in the shorter wavelength region between 300 and 360 nm is primarily attributed to the higher transmission capability of the silver layers. The near-zero passband observed between wavelengths of 400 and 480 nm is associated with the thickness of the dielectric layer. Furthermore, the peak position correlates with the number of layers, as illustrated by the patterns in the figure.

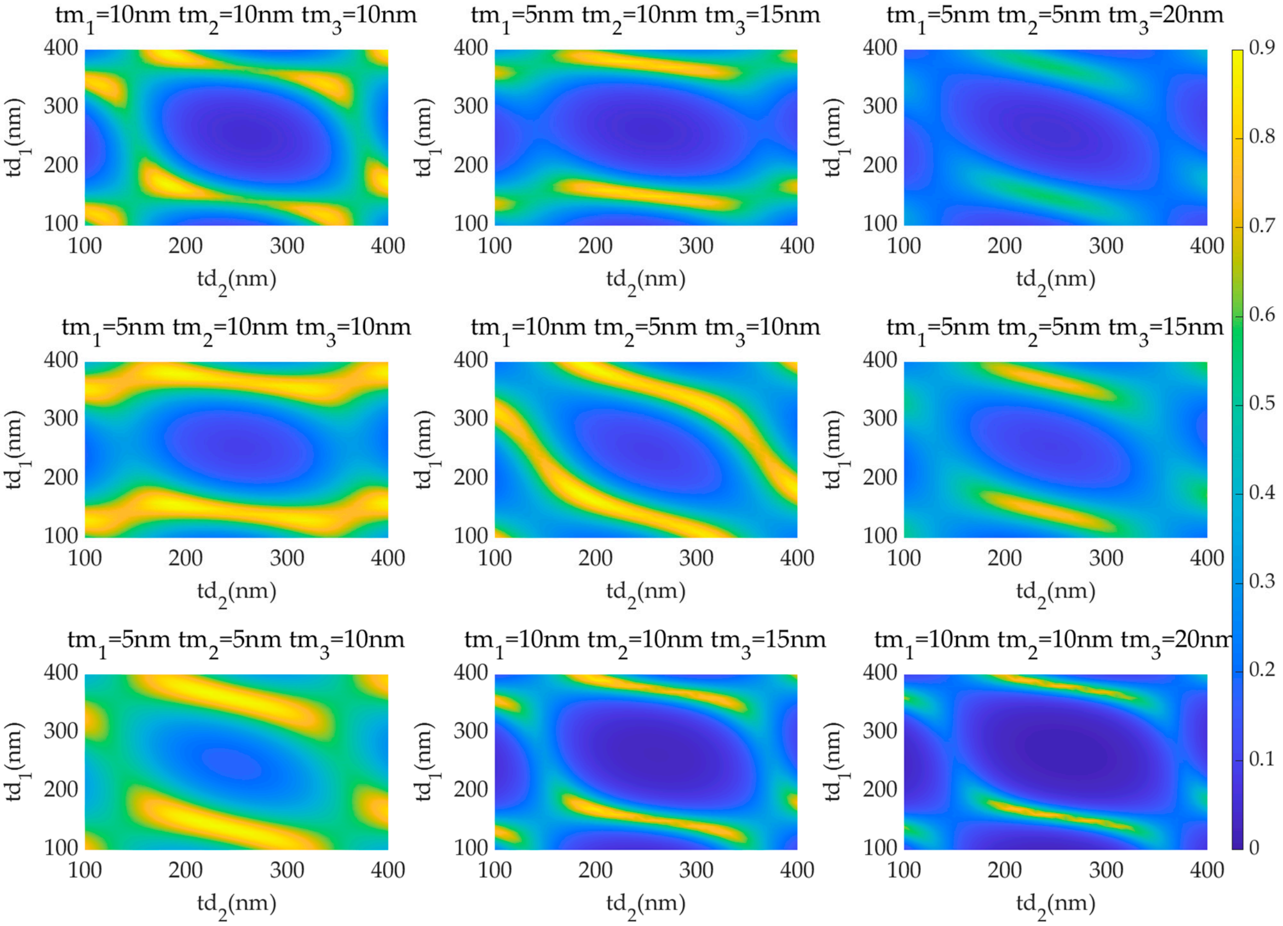

Figure 6. Transmittance of the multilayer structure with n = 3 at 640 nm, depending on the thickness of the dielectric layers with the corresponding thickness of the silver layer.

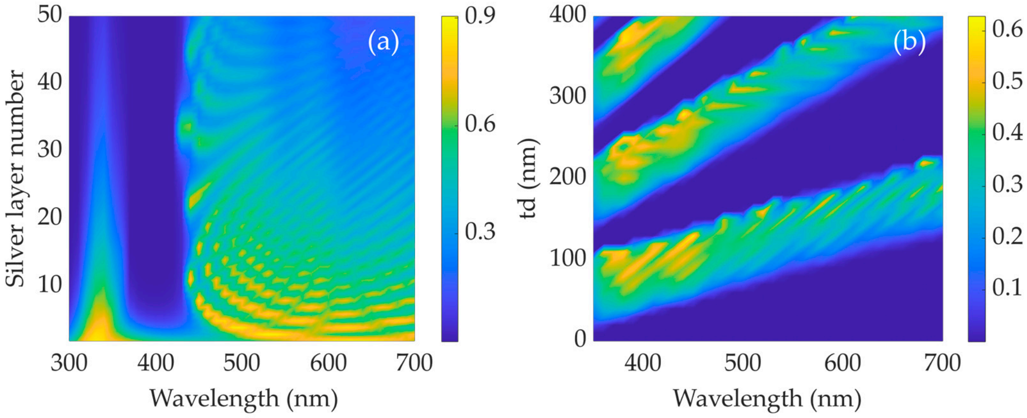

Figure 7. Transmittance of a silver–dielectric multilayer structure: (**a**) variance in transmittance with the number of layers and the wavelength when tm = 10 nm and td = 130 nm; (**b**) variance in transmittance with the dielectric layer thickness and the wavelength when tm = 15 nm and n = 20.

Simultaneously, the passband of the structure broadens with an increase in the number of layers, as evidenced by a comparative analysis of Figures 2a,b and 7b. The slope of the phase delay at various levels exhibits a variation pattern analogous to that observed in structures with two or three metal layers. Moreover, the peak-to-valley ratio can be modulated through adjustments in the thickness of the metal layer; precisely, a thinner metal layer corresponds to a lower ratio.

Conversely, if the thickness of the silver layer is increased further, the peak-to-valley ratio also increases, yielding a comb-like filter. The positions and widths of the comb's teeth are arranged in an arithmetic sequence, as illustrated in Figure 8a. Narrowing the passband of the comb-like pattern can be achieved by incorporating additional layers with varying dielectric thicknesses (td). Consequently, the number of comb teeth can be controlled. As demonstrated in Figure 8b, the thinnest FWHM of the filter is reduced to 2 nm, corresponding to the peak located furthest to the left on the curve. The transmittance decreases with an increase in each metallic layer due to the intrinsic of the material. Both the transmission efficiency and the width of the peaks can be further modulated by adjusting the number of layers (j), the thickness of the metal layer (tm), the thickness of the dielectric layer (td), and the phase level (*l*). Meanwhile, the transmittance of the structure with 20 metallic layers can be modulated to be higher than 50% when the total thickness of the metallic layers is thicker than 200 nm.

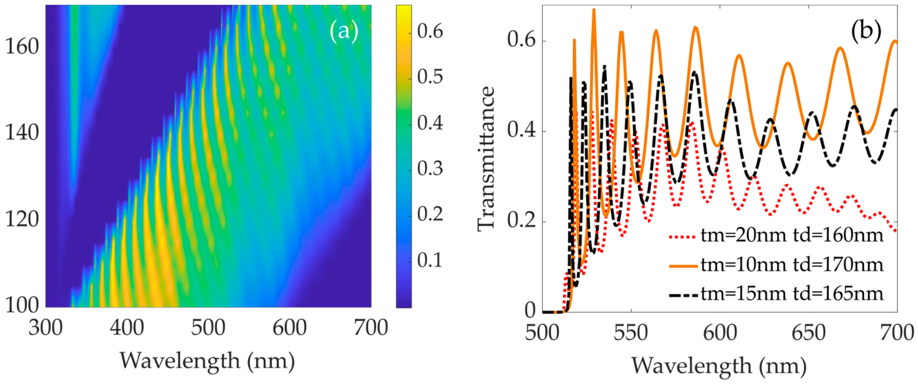

Figure 8. Transmittance of a multilayer structure with n = 20, depending on the wavelength: (**a**) tm = 15; (**b**) comparisons with metal films of different thicknesses.

Building upon the preceding results and analysis, we propose an idealized scenario involving the systematic variation of the metal layers' thickness alongside readily fabricable and controllable parameters. In this idealized scenario, the thickness of the silver layer is set to increment in an arithmetic sequence, ranging from 1 to 5 nm or even up to 10 nm. Consequently, the passband is broadened and smoothed, achieving uniform coverage across the entire visible spectrum, with a transmittance of approximately 80% as plotted in Figure 9a. The profile of the curve can be further refined by varying the thickness of the dielectric layer (*td*) or implementing a random distribution of both the metal and dielectric layers' thicknesses, thereby allowing for the smoothing or sharpening of the curve as required as shown in Figure 9b.

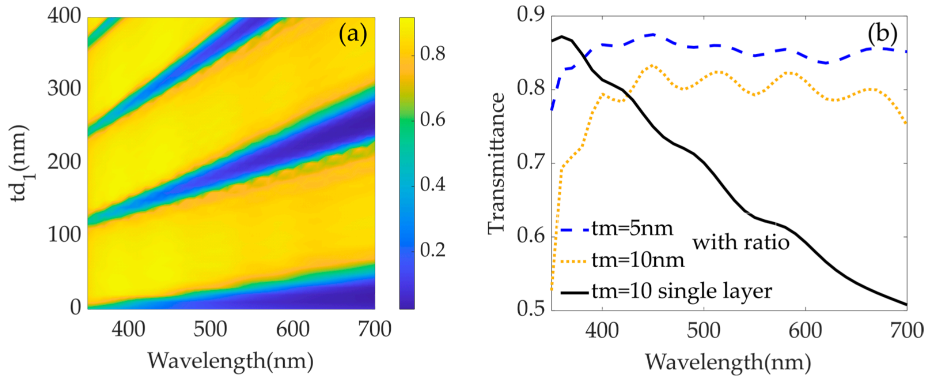

Figure 9. Transmittance of the structure with 10 metal layers with a metal variation ratio of 0.1: (**a**) metal films with a thickness from 1 nm to 5 nm; (**b**) comparisons between the multilayer structure with td = 100 nm and the single-layer structure.

4. Conclusions and Discussion

Our study focuses on the improvement of the transmittance of metamaterials with metal components. A solution that adds additional layers was designed to form a multilayer structure with vertical cavities. Therefore, the electronic waves can be strengthened during interference. A simplified equation is proposed to predict the structural parameters. The properties of transmittance with multilayer structures comprising metal and dielectric layers at the visible spectrum are numerically and analytically discussed.

Furthermore, by varying the thicknesses of these layers, it is possible to achieve a refined control over the passband, peak positions, and overall transmittance. An idealized scenario is proposed, where the thickness of the silver layers is systematically varied in an arithmetic sequence, leading to a smooth and broad passband covering the visible spectrum with a transmittance of around 80%. Additionally, the peak-to-valley ratio can be adjusted by changing the metal layers' thickness, and the formation of comb-like filters can be achieved, with the number of comb teeth being controlled by the additional layers with varying dielectric thicknesses. The ability to finely tune the transmittance characteristics of multilayer structures through controlled variations in the layers' thickness presents significant implications for applications requiring precise optical filtering. The observed dependence of the passband and peak positions on the thickness of the layers suggests that such structures could be optimized for specific spectral ranges, including but not limited to the visible spectrum. The comb-like filters, characterized by their arithmetic sequences of peak positions and widths, offer potential applications in areas requiring selective light transmission, such as sensor technologies or advanced optical devices. Further modifications, such as random distributions of the layers' thicknesses, could lead to the development of more sophisticated optical components designed to meet specific performance criteria. However, for multilayer structures, a number of parameters need to be optimized due to the interaction between different layers and the nonlinear distribution of the transmittance and peak position. To alleviate the associated workload, we are planning to try a machine learning algorithm to explore an inverse design method.

Nevertheless, the parameters chosen in the simulation have taken the possibilities of fabrication with the existing facilities, though only numerical results are presented. Thermal or electron beam (E-beam) evaporation is recommended due to the thinness of the film, with which a good match between the experimental and numerical results has been obtained for a thin silver film [33,34]. Continuous metallic films can be fabricated by controlling the evaporation rate and the degree of vacuum. For the dielectric layer, E-beam evaporation can be utilized for the deposition of materials such as aluminum oxide (Al_2O_3) or magnesium fluoride (MgF_2), which possess a refractive index similar to that assumed in our manuscript. However, when the thickness increases to micrometers across multiple layers, the workload involved in measuring the thickness during evaporation becomes substantial. An alternative method known as spin-coating is suggested, which allows for the fabrication of dielectric films using materials such as spin-on glass (SOG, Futurrex, Inc., Franklin, NJ, USA) on a substrate. The thickness can be controlled by adjusting the rotational velocity or the solvent's concentration. Both the metallic and dielectric films' thicknesses can be measured using atomic force microscopy (AFM) or Dektak profilometry for a double check. With regard to transmittance, the normalized spectrum can be measured using Fourier transform infrared spectroscopy (FTIR).

Thin metal films induce the generation of surface plasmons on both the upper and lower surfaces upon interaction with the incident beam, a phenomenon that can also be observed from the splitting of the transmittance enhancement line in Figure 4b. Meanwhile, the multilayer structure is capable of achieving polarization modulation and phase delay.

Preliminary results are presented in Figure 10. A simple structure consisting of a slit array, with a slit width w and a period p, is incorporated into the multilayer structure. The added structure leads to anisotropic distribution. Therefore, the transmittance varies according to the direction of polarization. Figure 1a illustrates the comparison between the transmittance along (Ts) and perpendicular (Tp) to the slits' direction. An extinction ratio of 20 is achieved, which is smaller than the existing structures but can be further improved by optimizing structural parameters, such as increasing the aspect ratio of the slits.

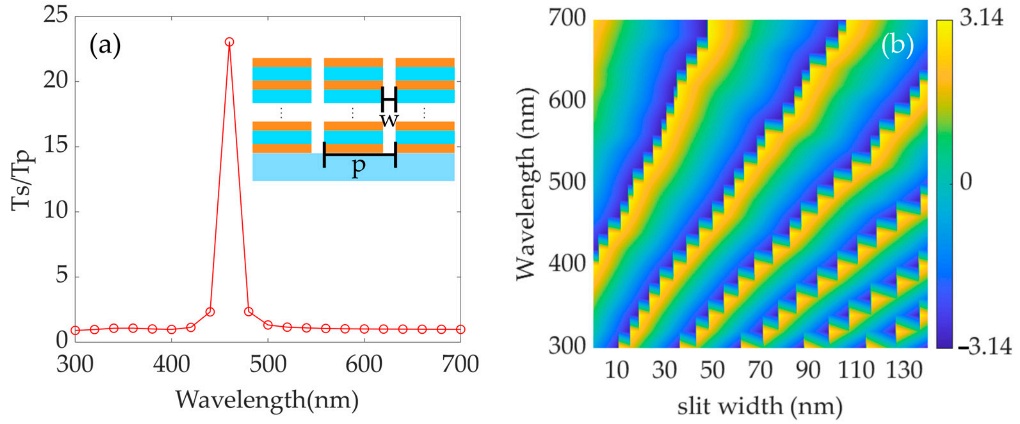

Figure 10. Layered structure with air slits: (**a**) polarization when td = 100 nm, tm_1 = 15 nm, tm_2 = 15 nm, tm_3 = 10 nm, w = 100, and p = 400 nm; (**b**) phase delay when td = 100 nm and tm_1 = tm_2 = 20 nm.

If the width of the slits is incremented in an arithmetic sequence from 10 nm to 130 nm with a step of 10 nm, the phase delay, depending on the wavelength and the slits' width are plotted in Figure 10 with the p-polarized incident wave. If the slits are replaced with holes, the variation in the phase delay with respect to the width and wavelength becomes evident. This characteristic renders the structure suitable for the design of flat plasmonic lenses by mimicking the phase delay of a traditional lens. However, it must be acknowledged that this manuscript focuses primarily on the detailed discussion of transmittance. The structural parameters require further optimization for real-world applications of multi-layer structures with diverse functionalities, and the predictions need validation through additional experimental demonstrations.

Author Contributions: Conceptualization, H.L. and G.C.; methodology, H.L.; software, H.L.; validation, H.L., L.Z. and G.H.; formal analysis, H.L.; investigation, H.L.; resources, H.L. and Z.Z.; data curation, H.L.; writing—original draft preparation, H.L.; writing—review and editing, G.C.; visualization, H.L.; supervision, Z.Z.; project administration, H.L.; funding acquisition, H.L., G.C., G.H. and Z.Z. All authors have read and agreed to the published version of the manuscript.

Funding: This research was funded by the R&D Program of Beijing Municipal Education Commission (grant number KM202211232018), the Young Backbone Teacher Support Plan of Beijing Information Science &Technology University (grant number YBT 202412), the National Natural Science Foundation of China (grant number 62105036), and Anhui Key Laboratory of Industrial Wastewater and Environmental Treatment Open Subjects (grant number DHSZ202304).

Data Availability Statement: Data are available upon request.

Conflicts of Interest: The authors declare no conflicts of interest.

References

1. Wu, B.; Monks, J.N.; Yue, L.; Hurst, A.; Wang, Z. Optimized Wide-Angle Metamaterial Edge Filters: Enhanced Performance with Multilayer Designs and Antireflection Coatings. *Photonics* **2024**, *11*, 446. [CrossRef]
2. Kong, Y.B.; Sun, X.Y.; Chen, W.W.; Xu, S.T.; Liu, G.Q.; Wang, Y.H. Multi-Band Spin-Selective Transmission and Reflection in Bi-Layer T-Shaped Metamaterial. *Results Phys.* **2023**, *54*, 107075. [CrossRef]
3. Du, C.; Zhou, D.; Guo, H.H.; Pang, Y.Q.; Shi, H.Y.; Liu, W.F.; Su, J.Z.; Singh, C.; Trukhanov, S.; Trukhanov, A.; et al. An Ultra-Broadband Terahertz Metamaterial Coherent Absorber Using Multilayer Electric Ring Resonator Structures Based on Antireflection Coating. *Nanoscale* **2020**, *12*, 9769–9775. [CrossRef] [PubMed]
4. Hu, J.; Bandyopadhyay, S.; Liu, Y.H.; Shao, L.Y. A Review on Metasurface: From Principle to Smart Metadevices. *Front. Phys.* **2021**, *8*, 586087. [CrossRef]

5. Pakizeh, T.; Abrishamian, M.S.; Granpayeh, N.; Dmitriev, A.; Käll, M.; Barnes, W.L.; Dereux, A.; Ebbesen, T.W.; Cai, W.; Chettiar, U.K.; et al. *Exeprimental Demonstration of Near-Infrared Negative-Index Metamaterials*; IEEE Press: Piscataway, NJ, USA, 2003; Volume 424.
6. Li, H.; Wang, Y.; Chen, G. The Design of a Beam Shaping Lens with Flat Surfaces and Ultra-Thin Thickness to Convert a Gaussian Beam to a Top-Hat Beam. In Proceedings of the Thirteenth International Conference on Information Optics and Photonics (CIOP 2022), Xi'an, China, 15 December 2022; p. 131.
7. Patel, S.K.; Surve, J.; Parmar, J.; Katkar, V.; Jadeja, R.; Taya, S.A.; Ahmed, K. Graphene-Based Metasurface Solar Absorber Design for the Visible and near-Infrared Region with Behavior Prediction Using Polynomial Regression. *Optik* **2022**, *262*, 169298. [CrossRef]
8. Ming Qing, Y.; Feng Ma, H.; Wei Wu, L.; Jun Cui, T. Manipulating the Light-Matter Interaction in a Topological Photonic Crystal Heterostructure. *Opt. Express* **2020**, *28*, 34904. [CrossRef]
9. Wang, H.; Hu, Z.; Deng, J.; Zhang, X.; Chen, J.; Li, K.; Li, G. All-Optical Ultrafast Polarization Switching with Nonlinear Plasmonic Metasurfaces. *Sci. Adv.* **2024**, *10*, eadk3882. [CrossRef]
10. Khorasaninejad, M.; Capasso, F. Metalenses: Versatile Multifunctional Photonic Components. *Science* **2017**, *358*, eaam8100. [CrossRef]
11. Chen, J.H.; Zheng, B.C.; Shao, G.H.; Ge, S.J.; Xu, F.; Lu, Y.Q. An All-Optical Modulator Based on a Stereo Graphene-Microfiber Structure. *Light Sci. Appl.* **2015**, *4*, e360. [CrossRef]
12. Barulin, A.; Kim, I. Hyperlens for capturing sub-diffraction nanoscale single molecule dynamics. *Opt. Express* **2023**, *31*, 12162–12174. [CrossRef]
13. Qing, Y.M.; Ma, H.F.; Ren, Y.Z.; Yu, S.; Cui, T.J. Near-Infrared Absorption-Induced Switching Effect via Guided Mode Resonances in a Graphene-Based Metamaterial. *Opt. Express* **2019**, *27*, 5253. [CrossRef] [PubMed]
14. Lim, S.W.D.; Meretska, M.L.; Capasso, F. A High Aspect Ratio Inverse-Designed Holey Metalens. *Nano Lett.* **2021**, *21*, 8642–8649. [CrossRef] [PubMed]
15. Wu, K.; Liu, J.J.; Ding, Y.j.; Wang, W.; Liang, B.; Cheng, J.C. Metamaterial-Based Real-Time Communication with High Information Density by Multipath Twisting of Acoustic Wave. *Nat. Commun.* **2022**, *13*, 5171. [CrossRef]
16. Patel, S.K.; Wekalao, J.; Alsalman, O.; Surve, J.; Parmar, J.; Taya, S.A. Development of Surface Plasmon Resonance Sensor with Enhanced Sensitivity for Low Refractive Index Detection. *Opt. Quantum Electron.* **2023**, *55*, 1001. [CrossRef]
17. Gan, X.; Zhao, C.; Wang, Y.; Mao, D.; Fang, L.; Han, L.; Zhao, J. Graphene-Assisted All-Fiber Phase Shifter and Switching. *Optica* **2015**, *2*, 468. [CrossRef]
18. Chen, K.; Zhou, X.; Cheng, X.; Qiao, R.; Cheng, Y.; Liu, C.; Xie, Y.; Yu, W.; Yao, F.; Sun, Z.; et al. Graphene Photonic Crystal Fibre with Strong and Tunable Light–Matter Interaction. *Nat. Photonics* **2019**, *13*, 754–759. [CrossRef]
19. Tang, W.; Dai, J.Y.; Chen, M.; Li, X.; Cheng, Q.; Jin, S.; Wong, K.K.; Cui, T.J. Programmable Metasurface-Based RF Chain-Free 8PSK Wireless Transmitter. *Electron. Lett.* **2019**, *55*, 417–420. [CrossRef]
20. Dhama, R.; Yan, B.; Palego, C.; Wang, Z. Super-Resolution Imaging by Dielectric Superlenses: TiO_2 Metamaterial Superlens versus Batio3 Superlens. *Photonics* **2021**, *8*, 222. [CrossRef]
21. Li, H.; Fu, L.; Frenner, K.; Osten, W. Design Studies of a Far-Field Plasmonic Superlens with an Enlarged Field of View. *Opt. Mater.* **2023**, *138*, 113688. [CrossRef]
22. Guo, Z.; Jiang, H.; Chen, H. Hyperbolic Metamaterials: From Dispersion Manipulation to Applications. *J. Appl. Phys.* **2020**, *127*, 071101. [CrossRef]
23. Joo, W.-J.; Kyoung, J.; Esfandyarpour, M.; Lee, S.-H.; Koo, H.; Song, S.; Kwon, Y.-N.; Ho Song, S.; Cheol Bae, J.; Jo, A.; et al. Metasurface-Driven OLED Displays beyond 10,000 Pixels per Inch. *Science* **2020**, *370*, 459–463. [CrossRef] [PubMed]
24. Li, T.; Nagal, V.; Gracias, D.H.; Khurgin, J.B. Limits of Imaging with Multilayer Hyperbolic Metamaterials. *Opt. Express* **2017**, *25*, 13588. [CrossRef] [PubMed]
25. Liu, F.; Wang, D.; Zhu, H.; Zhang, X.; Liu, T.; Sun, S.; Zhang, X.; He, Q.; Zhou, L. High-Efficiency Metasurface-Based Surface-Plasmon Lenses. *Laser Photonics Rev.* **2023**, *17*, 2201001. [CrossRef]
26. Li, J.; Yuan, Y.; Yang, G.; Wu, Q.; Zhang, W.; Burokur, S.N.; Zhang, K. Hybrid Dispersion Engineering Based on Chiral Metamirror. *Laser Photonics Rev.* **2023**, *17*, 2200777. [CrossRef]
27. Wang, Y.; Xiao, Y.; Zhao, X.; Wen, D. Fabrication and Characterization of Monolithic Integrated Three-Axis Acceleration/Pressure/Magnetic Field Sensors. *Micromachines* **2024**, *15*, 412. [CrossRef]
28. Yin, X.; Zhu, H.; Guo, H.; Deng, M.; Xu, T.; Gong, Z.; Li, X.; Hang, Z.H.; Wu, C.; Li, H.; et al. Hyperbolic Metamaterial Devices for Wavefront Manipulation. *Laser Photonics Rev.* **2018**, *13*, 1800081. [CrossRef]
29. Wu, F.; Lu, G.; Guo, Z.; Jiang, H.; Xue, C.; Zheng, M.; Chen, C.; Du, G.; Chen, H. Redshift Gaps in One-Dimensional Photonic Crystals Containing Hyperbolic Metamaterials. *Phys. Rev. Appl.* **2018**, *10*, 064022. [CrossRef]
30. Moharam, M.G.; Grann, E.B.; Pommet, D.A.; Gaylord, T.K. Formulation for Stable and Efficient Implementation of the Rigorous Coupled-Wave Analysis of Binary Gratings. *JOSA A* **1995**, *12*, 1068–1076. [CrossRef]
31. Moharam, M.G.; Pommet, D.A.; Grann, E.B.; Gaylord, T.K. Stable Implementation of the Rigorous Coupled-Wave Analysis for Surface-Relief Gratings: Enhanced Transmittance Matrix Approach. *JOSA A* **1995**, *12*, 1077–1086. [CrossRef]
32. Koelling, D.; Freeman, A.; Mueller, F.; Johnson, P.B.; Christy, R.W. Optical Constants of the Noble Metals. *Phys. Rev. B* **1963**, *11*, 541.

33. Li, H.; Fu, L.; Frenner, K.; Osten, W. Cascaded DBR plasmonic cavity lens for far-field subwavelength imaging at a visible wavelength. *Opt. Express* **2018**, *26*, 19574–19582. [CrossRef] [PubMed]
34. Li, H.; Fu, L.; Frenner, K.; Osten, W. Cascaded Plasmonic Superlens for Far-Field Imaging with Magnification at Visible Wavelength. *Opt. Express* **2018**, *26*, 10888. [CrossRef] [PubMed]
35. Axelevitch, A.; Gorenstein, B.; Golan, G. Investigation of Optical Transmission in Thin Metal Films. *Phys. Procedia* **2012**, *32*, 1–13. [CrossRef]